36. M. N. Obrovac, L. Christensen, *Electrochem. Solid-State Lett.* **7**, A93–A96 (2004).

Acknowledgments: The tomography experiments were performed on the Tomographic Microscopy and Coherent Radiology Experiments (TOMCAT) beamline at the Swiss Light Source, Paul Scherrer Institut, Villigen, Switzerland. We thank P. Modregger, L. Nowack, and M.-F. Lagadec for their support during the beamtime; K. Kunze and W. Woodford for insightful discussion; D. Norris for access to SEM; and O. Waser and S. Pratsinis for access to XRD. We gratefully acknowledge material donations from TIMCAL and Arkema.

Supplementary Materials
www.sciencemag.org/content/342/6159/716/suppl/DC1
Materials and Methods
Supplementary Text
Figs. S1 to S3
Table S1
References (*37*, *38*)
Movies S1 to S4

13 June 2013; accepted 3 October 2013
Published online 17 October 2013;
10.1126/science.1241882

The Role of Surface Oxygen in the Growth of Large Single-Crystal Graphene on Copper

Yufeng Hao,[1] M. S. Bharathi,[2] Lei Wang,[3] Yuanyue Liu,[4] Hua Chen,[5] Shu Nie,[6] Xiaohan Wang,[1] Harry Chou,[1] Cheng Tan,[1] Babak Fallahazad,[7] H. Ramanarayan,[2] Carl W. Magnuson,[1] Emanuel Tutuc,[7] Boris I. Yakobson,[4] Kevin F. McCarty,[6] Yong-Wei Zhang,[2] Philip Kim,[8] James Hone,[3] Luigi Colombo,[9]* Rodney S. Ruoff[1]*

The growth of high-quality single crystals of graphene by chemical vapor deposition on copper (Cu) has not always achieved control over domain size and morphology, and the results vary from lab to lab under presumably similar growth conditions. We discovered that oxygen (O) on the Cu surface substantially decreased the graphene nucleation density by passivating Cu surface active sites. Control of surface O enabled repeatable growth of centimeter-scale single-crystal graphene domains. Oxygen also accelerated graphene domain growth and shifted the growth kinetics from edge-attachment–limited to diffusion-limited. Correspondingly, the compact graphene domain shapes became dendritic. The electrical quality of the graphene films was equivalent to that of mechanically exfoliated graphene, in spite of being grown in the presence of O.

Control of the nucleation and growth of graphene during the chemical vapor deposition (CVD) process is important to achieve large, high-quality single crystals (*1*–*5*). Much attention has been paid to the process details, with emphasis on the parameters of carbon (C) precursors, hydrogen (H), copper (Cu), temperature, and pressure (*6*). As such, tuning the C:H ratio (*6*), changing the hydrocarbon and H_2 gas pressures (*7*), and smoothing the Cu surface before growth (*8*, *9*) have been used to grow graphene with desirable quality. However, the wide variation in domain size, shape, and film quality from lab to lab suggests that crucial growth parameters still remain unknown or uncontrolled. We show that oxygen (O) on the Cu surface not only suppresses graphene nucleation, fostering growth of ultralarge single-crystal graphene domains, but also lowers the C species edge attachment barrier and shifts the graphene domain shapes from compact to dendritic (*10*). First-principles calculations and phase field simulations provided a deeper insight into the proposed growth mechanism and reproduced the observed domain shapes.

Oxygen impurities were found to exist at different concentrations across commercially available Cu foils. Time-of-flight secondary ion mass spectrometry (TOF-SIMS) depth profile results [fig. S2B, see supplementary materials (*11*)] show that, for two different types of Cu foils, the O concentrations are ~10^{-2} and ~10^{-6} atomic % (the latter approaching the detection limit), hereafter referred to as "oxygen-rich Cu" (OR-Cu) and "oxygen-free Cu" (OF-Cu), respectively. When the two types of Cu were used to grow graphene under the same conditions in low-pressure CVD, the domain density for OR-Cu was ~0.9 mm^{-2}, more than three orders of magnitude lower than that for OF-Cu, which was about 2×10^3 mm^{-2} (Fig. 1, A and B). We also observed that graphene domains on OR-Cu always exhibited dendritic growth fronts, i.e., multibranched and rough domain edges (Fig. 1A, inset), whereas graphene domains on OF-Cu were compact with sharp edges (Fig. 1B, inset). When we exposed OF-Cu to O_2 [partial pressure of O_2 (P_{O_2}) = 1×10^{-3} torr; the substrates are defined as "OF-Cu (O)" hereafter] for 1 min before introducing methane (CH_4, $P_{CH_4} = 1 \times 10^{-3}$ torr), the resulting graphene growth yielded a low density of nuclei, ~6 mm^{-2}, and dendritic growth fronts (Fig. 1C) similar to those on OR-Cu. In addition, TOF-SIMS results (fig. S2A) showed the presence of surface O after O_2 exposure and annealing in H_2 (P_{H_2} = 0.1 torr). Because graphene growth on Cu is a surface-mediated process (*12*), it is reasonable that surface O species, either segregated out of the Cu bulk or adsorbed from O_2 exposure, participate in surface reactions and are thus responsible for the domain growth characteristics. Both experimental (*13*, *14*) and theoretical studies (*15*) have established that metal surface imperfections, such as step edges, defects, impurities, etc., can be active sites for graphene nucleation because of higher *d*-band centers at these lower-coordination sites, which lead to strong binding to adsorbates (*16*, *17*). For the same reasons, these active sites are also sinks for O. Thus, surface O on the Cu, regardless

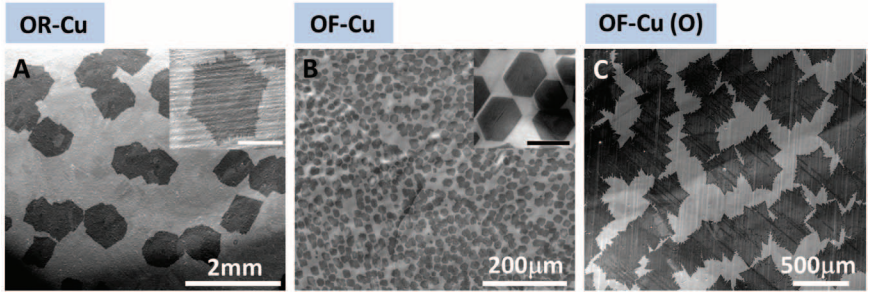

Fig. 1. The effect of O on graphene nucleation density and domain shapes on Cu. Scanning electron microscope (SEM) images of graphene domains grown on (**A**) OR-Cu, (**B**) OF-Cu, and (**C**) OF-Cu (O), respectively. In all cases, the $P_{CH_4} = 1 \times 10^{-3}$ torr, and P_{H_2} = 0.1 torr, and the growth time was 150 min for (A) and (C) and 50 min for (B). The insets in (A) and (B) are the high-magnification SEM images in each case. The scale bar is 500 μm in the inset of (A) and 20 μm in the inset of (B).

[1]Department of Mechanical Engineering and the Materials Science and Engineering Program, The University of Texas at Austin, Austin, TX 78712, USA. [2]Institute of High Performance Computing, A*STAR, 138632, Singapore. [3]Department of Mechanical Engineering, Columbia University, New York, NY 10027, USA. [4]Department of Mechanical Engineering and Materials Science, and Department of Chemistry, Rice University, Houston, TX 77005, USA. [5]Department of Physics, The University of Texas at Austin, Austin, TX 78712, USA. [6]Sandia National Laboratories, Livermore, CA 94550, USA. [7]Microelectronics Research Center, The University of Texas at Austin, Austin, TX 78758, USA. [8]Department of Physics, Columbia University, New York, NY 10027, USA. [9]Texas Instruments, Dallas, TX 75243, USA.

*Corresponding author. E-mail: r.ruoff@mail.utexas.edu (R.S.R); colombo@ti.com (L.C.)

of its source, effectively passivated the surface active sites where hydrocarbon accumulation would otherwise have taken place.

In order to further suppress graphene nucleation on Cu, we exposed the Cu substrates to varying amounts of O_2 ($P_{O_2} = 1 \times 10^{-3}$ torr) by simply increasing the exposure time up to 5 min before introducing CH_4. Typically, 2 min of O_2 exposure on OR-Cu can decrease the nucleation density to ~0.03 mm^{-2} (Fig. 2A). With longer O_2 exposure (5 min), the graphene nucleation density was as low as ~0.01 mm^{-2}, and individual domains grew to a diameter larger than 1 cm after a 12-hour growth period at $P_{CH_4} = 1 \times 10^{-3}$ torr (Fig. 2B). The same experiments with OF-Cu

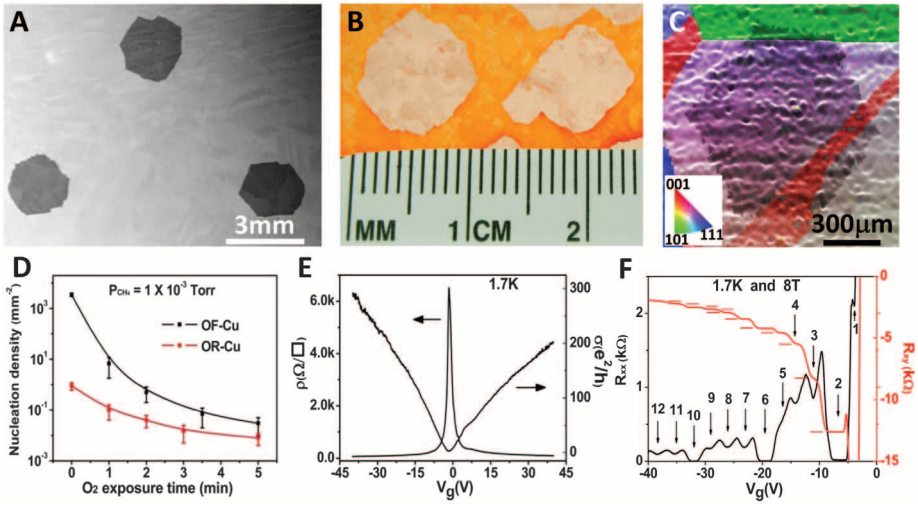

Fig. 2. Size, structure, and electrical transport properties of large graphene domains grown on Cu exposed to O_2. (**A**) SEM image of low-density graphene domains on OR-Cu exposed to O_2. (**B**) Optical image of centimeter-scale graphene domains on OR-Cu exposed to O_2. The sample was prepared by heating in air at 180°C for 30 min to oxidize bare Cu (orange) and visualize graphene domains (pale area), as reported by Wang *et al*. (*9*). (**C**) Superimposed SEM and EBSD images of a graphene domain grown across Cu multigrains. (**D**) The graphene nucleation density as a function of O_2 exposure time. (**E**) Plots of resistivity and conductivity as a function of gate voltage at 1.7 K. (**F**) Longitudinal resistivity, R_{xx}, measured on left axis (black) and Hall resistance, R_{xy}, on right axis (red) as a function of V_g.

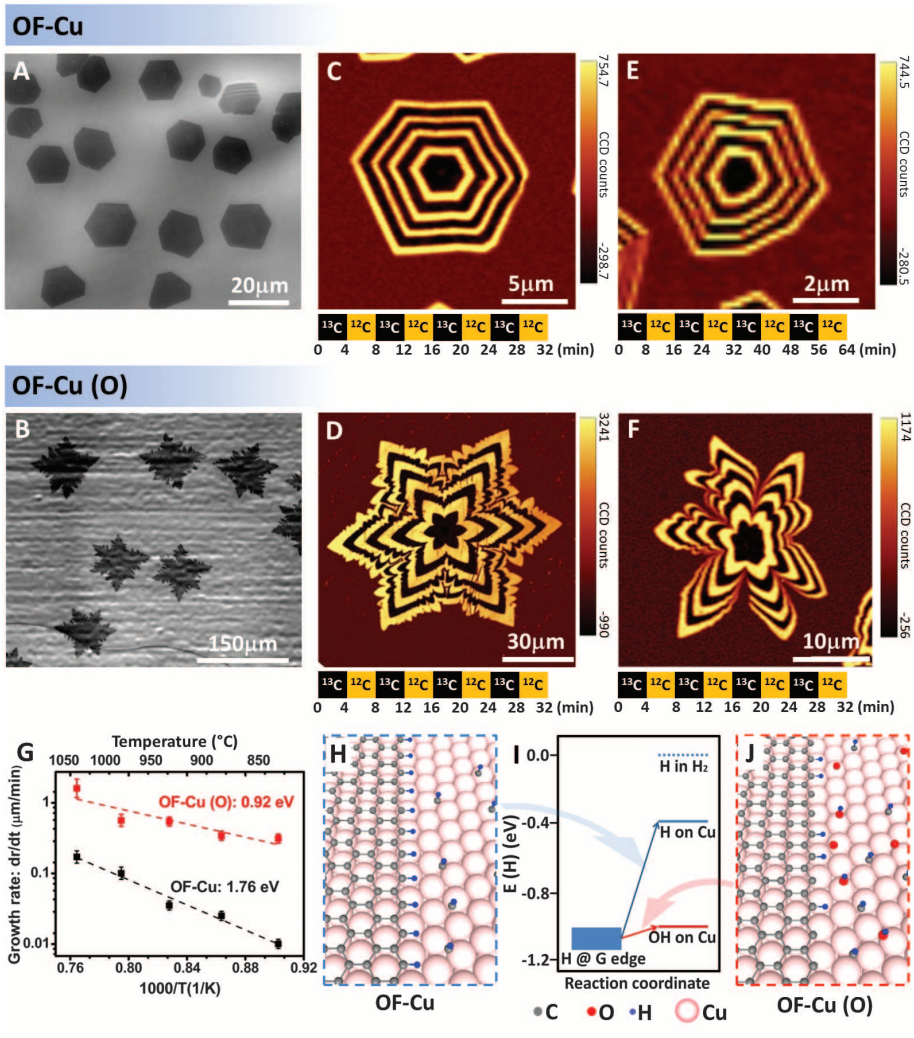

Fig. 3. The effect of O on graphene growth kinetics. SEM images of graphene domains grown on (**A**) OF-Cu and (**B**) OF-Cu (O). Isotope-labeled Raman maps of the 2D (G′) band intensities on Si substrates for growth at (**C** and **D**) 1035°C and (**E** and **F**) 885°C. The isotope switching intervals are indicated below each image. (**G**) Logarithmic plots of graphene domain growth rate $d\bar{r}/dt$ versus 1/T. The error bars are from calculations of different domains for each case, and the activation energy E_a is extracted from the slope of the linear fit. (**J** and **H**) Atomic-scale schematics of graphene edge growth on Cu with and without the assistance of O, respectively. (**I**) DFT calculated energies of different configurations of H attachment, in reference to H in H_2. The energy spread of H at the graphene edge is due to the computational uncertainty resulting from the lattice mismatch between graphene and Cu.

gave rise to a similar trend; i.e., the nucleation density decreased with increasing O_2 exposure time (Fig. 2D). Oxygen exposure provided a convenient tuning parameter for suppressing graphene nucleation and growing large domains. We used electron backscatter diffraction (EBSD) to map the crystalline orientations of Cu grains under a graphene domain. The results show that large graphene domains normally grow across several Cu grains, which usually have a grain size smaller than a few millimeters even after annealing (Fig. 2C). Low-energy electron diffraction (LEED) patterns (fig. S8) taken at different positions on the same domain show that, even though the underlying Cu is multigrain, all of the graphene diffraction patterns are aligned with each other, indicating a single-crystal graphene domain. LEED measurements were also performed on other randomly selected large graphene domains with varying shapes (such as in Fig. 2B) on multigrain Cu and confirmed that the domains are single crystals. These observations suggest that single-crystal Cu substrates are unnecessary to grow large single-crystal graphene films. In addition, we found that high growth temperatures and low P_{CH_4} facilitated single-crystal graphene growth. Raman spectra of the domains transferred onto silicon (Si) substrates confirmed that they are single-layer with no detectable defect-related D band (fig. S5).

Electrical- and magneto-transport measurements were then performed on Si (fig. S11) and hexagonal boron nitride (h-BN) substrates. Resistivity as a function of the back gate voltage of graphene films on h-BN (Fig. 2E) shows narrow and symmetric Dirac peaks with the charge neutrality point $V_g = -1.0$ V. The carrier mobility measured for three different samples ranged from 40,000 to 65,000 $cm^2\ V^{-1}\ s^{-1}$ at 1.7 K and from 15,000 to 30,000 $cm^2\ V^{-1}\ s^{-1}$ at room temperature when a carrier density–independent fitting method was used (*18*). Magneto-transport measurements show quantum Hall states at all integer filling factors from 1 to 12 at a magnetic field of 8 T (Fig. 2F), indicating that the fourfold degeneracy of the Landau levels is lifted. The onset of Shubnikov–de Haas oscillations was also observed at fields below 500 mT (fig. S12). These features suggest that the electrical quality of large graphene domains, despite having been grown with O on Cu, is among the best reported for CVD graphene (*19*) and comparable to that of micromechanically exfoliated graphene (*20*).

In addition to decreasing graphene nucleation density, O affected graphene growth kinetics. Figure 3A shows that graphene domains on OF-Cu were compact with a domain size of ~15 μm after 32 min of growth at 1035°C and $P_{CH_4} = 2 \times 10^{-3}$ torr. However, when graphene was grown on OF-Cu (O) ($P_{O_2} = 1 \times 10^{-3}$ torr, 30 s of exposure) under the same conditions and for the same growth time, the domain size increased to ~100 μm (Fig. 3B). This acceleration of graphene domain growth by surface O may seem counterintuitive, because O has been associated with C species oxidation and graphene etching (*21*). Oxygen also decreased the graphene film coverage on the Cu substrates by 5 to 10 times after 32 min of growth (*11*). This decrease resulted from the nucleation density on OF-Cu (O) being more than two orders of magnitude lower despite the higher individual domain growth rate (*11*).

We visualized the time evolution of domain growth at different growth temperatures with C isotope labeling and Raman mapping (Fig. 3, C to F, and fig. S7). Over a wide temperature range, the domains on OF-Cu remained compact hexagons as they grew, whereas on OF-Cu (O), the domains were always multibranched and dendritic. The consistent domain shapes suggest that the kinetics do not change throughout the growth. Also, the radial growth rates of individual domains were nearly constant along a given orientation, as measured by the widths of the isotopically labeled bands. We plotted the growth rate as a function of temperature (Fig. 3G). According to the Arrhenius equation $d\bar{r}/dt \propto \exp(-E_a/k_B T)$,

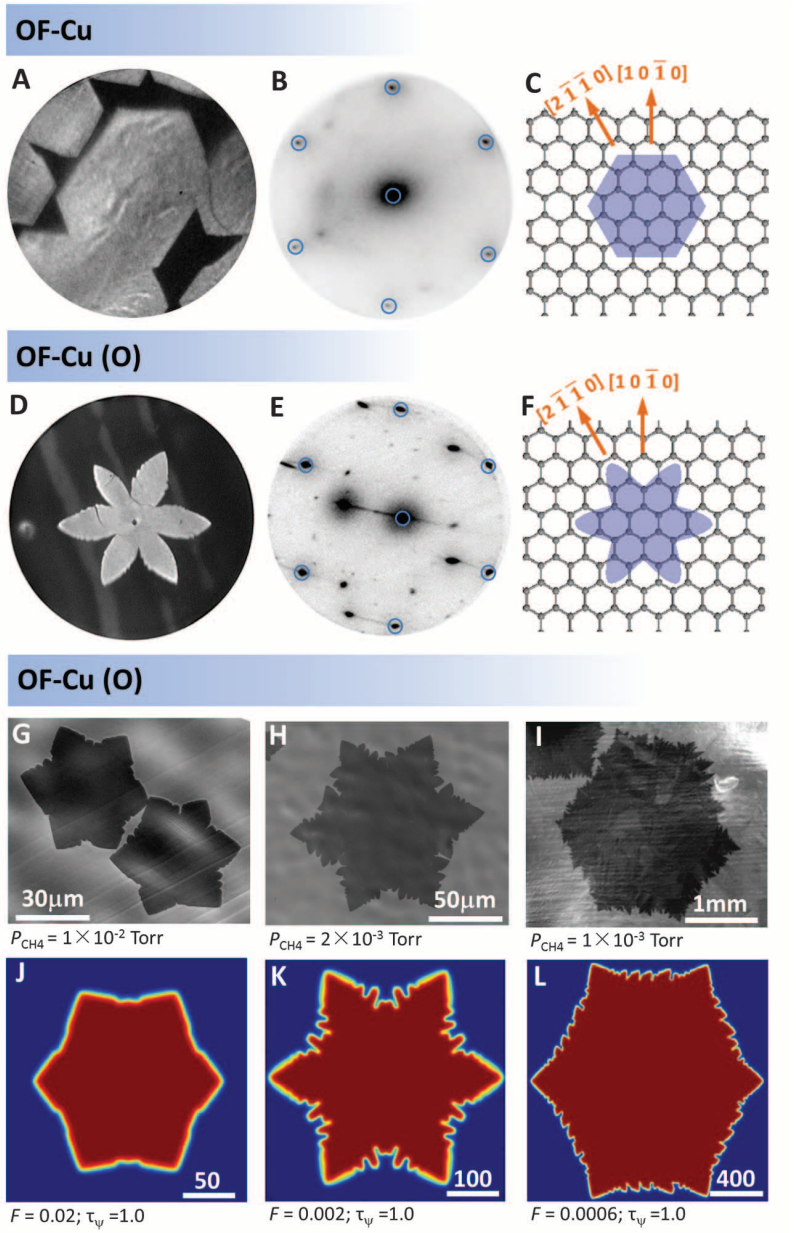

Fig. 4. The effect of O on graphene domain shapes on Cu. (**A**, **B**, **D**, and **E**) Low-energy electron microscopy images and corresponding LEED patterns (blue circles) of graphene domains on OF-Cu and OF-Cu (O), respectively. The extra LEED spots came from the faceted Cu. The viewing fields in (A) and (D) are 20 and 60 μm, respectively. (**C** and **F**) Schematics of growth directions of the two types of graphene domains. (**G** to **I**) SEM images of graphene domains grown on OF-Cu (O) as a function of P_{CH_4}. (**J** to **L**) Phase field simulation results as a function of characteristic attachment time and C flux. The scale bars in (J) to (L) refer to simulation units, corresponding to length.

where $\bar{r}$ is the average radius (*11*), E_a is the growth activation energy, k_B is the Boltzmann constant, and T is temperature. The value of E_a was 1.76 eV for graphene on OF-Cu and 0.92 eV on OF-Cu (O), indicating that, in the dynamic growth process, the barrier of the rate-limiting step is reduced.

For hydrocarbon (e.g., CH_4) conversion to graphene on Cu during CVD growth, the following elementary steps are expected (*3*, *22*, *23*): (i) CH_4 adsorption on Cu surfaces; (ii) CH_4 (partial-) dehydrogenation, resulting in C species such as CH_x ($x = 0$ to 3); (iii) surface diffusion of C species; and (iv) C species attachment to the graphene domain edge and incorporation into the graphene lattice. The dehydrogenation of CH_4 on Cu is endothermic (energetically unfavorable), and the diffusing C species on Cu are mainly CH_x ($0 < x < 4$), rather than atomic C (*22*). Density functional theory (DFT) calculations revealed that the H-terminated graphene edge on Cu is more energetically favorable than the bare graphene edge on Cu (Fig. 3, H and I). Thus, C species edge attachment and lattice incorporation require dehydrogenation [e.g., $CH_x \xrightarrow{Cu} CH_{x-1} + H$ (x = 4, 3, 2, 1)], which is considered rate-limiting (*3*, *22*, *23*). In contrast, theoretical studies have shown that preadsorbed O on the Cu surface can enhance the dissociation of hydrocarbons (Fig. 3J) through the reaction $CH_x + O \xrightarrow{Cu} CH_{x-1} + OH$ ($x = 4, 3, 2, 1$) (*24*, *25*). Our DFT calculations have shown that the energy of H in the form of an OH group on Cu is lower than that of H on Cu by 0.6 eV/H (Fig. 3I), pointing to a lower activation energy of edge dehydrogenation according to the Bell-Evans-Polanyi principle (*26*). Thus, experimental data from the isotope-labeled growth and the atomic-scale calculations reveal that O helps reduce the edge attachment barrier, facilitates C incorporation, and accelerates graphene growth. In the process, graphene growth proceeded by continuous C edge attachment and lattice incorporation, whereas surface O species were consumed and then desorbed. This scenario does not necessarily conflict with the passivation effect of O on graphene nucleation. The latter is governed by different kinetic processes (*23*) that typically require a much higher supersaturation density of C species than that during growth, in which dehydrogenation may not be the critical step.

The above model is supported by the change of graphene domain morphology with O_2 exposure. Here, we focus on the domains on Cu(111). Figure 4A shows the typical shape of graphene domains formed on OF-Cu: compact hexagons with sharp edges, as obtained from the kinetic Wulff construction (*27*), which is expected as a result of edge-attachment–limited growth. In contrast, graphene domains grown on OF-Cu (O) became multibranched or dendritic (Fig. 4D), which is typical of diffusion (mass transport)–limited growth (*3*, *28*). The morphology change indicates that, with the introduction of O, C attachment at domain edges is no longer rate-limiting, and domain growth is instead governed by C diffusion or equivalently C flux, in agreement with our observations and analysis. The corresponding LEED patterns (Fig. 4, B and E) show only one set of hexagonal diffraction patterns, indicating that both domains are single crystals. Figure 4, C and F, sketch the relationship between the domain shapes and the graphene lattice. Both domains exhibit fast growth in the $[2\bar{1}\bar{1}0]$ direction and slow growth in the $[10\ \bar{1}0]$ direction, consistent with previous work, in which hexagonal domains have been reported to have zigzag-terminated edges (*29*). Oxygen affected the domain shapes by modifying the growth kinetics but preserved the sixfold crystallographic symmetry. We further found that graphene domains on OF-Cu maintain a hexagonal shape when P_{CH_4} ranges from 1×10^{-3} to 5×10^{-2} torr (fig. S9). However, on OF-Cu (O), different domain shapes appear as a function of P_{CH_4} (Fig. 4, G to I). The sensitive dependence of domain morphology on C concentration again suggests that the growth kinetics has been brought into the diffusion-limited regime by O.

To test the proposed growth mechanisms, a phase field model was developed to examine the domain shape evolution (*11*). Two key parameters, namely the characteristic attachment time of C species (τ_ψ) and C flux (F, reflecting the P_{CH_4}) are varied to simulate the experimental conditions. The attachment time is closely related to the edge attachment barrier: The higher the energy barrier, the longer the characteristic attachment time. The symmetry of the graphene domains is dictated by the sixfold graphene edge energy, in agreement with experimental observations. The simulated domain shapes are shown in Fig. 4, J to L, and fig. S9. When τ_ψ is long, the domain shape is hexagonal even if F is changed within a large range; whereas when τ_ψ decreases, the hexagonal domain turns into a six-branched domain at the same F. Furthermore, at the low τ_ψ value, F becomes the dominant parameter and can tune the domain shapes from six-branched to dendritic. Thus, lowering the attachment barrier changes the domain shape in the same manner as O_2 exposure in experiments. Thus, a rich variety of graphene domain morphologies (*30*, *31*) can be explained and reproduced when the O effect is considered in the growth kinetics.

References and Notes

1. X. Li *et al.*, *Science* **324**, 1312–1314 (2009).
2. S. Bae *et al.*, *Nat. Nanotechnol.* **5**, 574–578 (2010).
3. N. C. Bartelt, K. F. McCarty, *MRS Bull.* **37**, 1158–1165 (2012).
4. A. W. Tsen *et al.*, *Science* **336**, 1143–1146 (2012).
5. P. M. Ajayan, B. I. Yakobson, *Nat. Mater.* **10**, 415–417 (2011).
6. S. Bhaviripudi, X. Jia, M. S. Dresselhaus, J. Kong, *Nano Lett.* **10**, 4128–4133 (2010).
7. I. Vlassiouk *et al.*, *ACS Nano* **5**, 6069–6076 (2011).
8. Z. Yan *et al.*, *ACS Nano* **6**, 9110–9117 (2012).
9. H. Wang *et al.*, *J. Am. Chem. Soc.* **134**, 3627–3630 (2012).
10. Z. Zhang, M. G. Lagally, *Science* **276**, 377–383 (1997).
11. Materials and methods are available as supplementary materials on *Science* Online.
12. X. Li, W. Cai, L. Colombo, R. S. Ruoff, *Nano Lett.* **9**, 4268–4272 (2009).
13. S. Nie, J. M. Wofford, N. C. Bartelt, O. D. Dubon, K. F. McCarty, *Phys. Rev. B* **84**, 155425 (2011).
14. G. H. Han *et al.*, *Nano Lett.* **11**, 4144–4148 (2011).
15. J. Gao, J. Yip, J. Zhao, B. I. Yakobson, F. Ding, *J. Am. Chem. Soc.* **133**, 5009–5015 (2011).
16. H. Chen, W. Zhu, Z. Zhang, *Phys. Rev. Lett.* **104**, 186101 (2010).
17. B. Hammer, J. K. Nørskov, *Adv. Catal.* **45**, 71–129 (2000).
18. E. H. Hwang, S. Adam, S. D. Sarma, *Phys. Rev. Lett.* **98**, 186806 (2007).
19. N. Petrone *et al.*, *Nano Lett.* **12**, 2751–2756 (2012).
20. C. R. Dean *et al.*, *Nat. Nanotechnol.* **5**, 722–726 (2010).
21. E. Starodub, N. C. Bartelt, K. F. McCarty, *J. Phys. Chem. C* **114**, 5134–5140 (2010).
22. W. Zhang, P. Wu, Z. Li, J. Yang, *J. Phys. Chem. C* **115**, 17782–17787 (2011).
23. H. Kim *et al.*, *ACS Nano* **6**, 3614–3623 (2012).
24. I. Alstrup, I. Chorkendorff, S. Ullmann, *Surf. Sci.* **264**, 95–102 (1992).
25. B. Xing, X. Y. Pang, G. C. Wang, *J. Catal.* **282**, 74–82 (2011).
26. R. A. van Santen, M. Neurock, S. G. Shetty, *Chem. Rev.* **110**, 2005–2048 (2010).
27. V. I. Artyukhov, Y. Liu, B. I. Yakobson, *Proc. Natl. Acad. Sci. U.S.A.* **109**, 15136–15140 (2012).
28. T. A. Witten Jr., L. M. Sander, *Phys. Rev. Lett.* **47**, 1400–1403 (1981).
29. Q. Yu *et al.*, *Nat. Mater.* **10**, 443–449 (2011).
30. B. Wu *et al.*, *NPG Asia Mater.* **5**, e36 (2013).
31. A. T. Murdock *et al.*, *ACS Nano* **7**, 1351–1359 (2013).

Acknowledgments: We thank V. B. Shenoy (University of Pennsylvania), Zhenyu Zhang [University of Science and Technology of China (USTC)], Zhenyu Li (USTC), N. C. Bartelt (Sandia Laboratories), P. Sutter (Brookhaven Laboratory), Gui-Chang Wang (Nankai University), Cheng Gong (University of Texas–Dallas), Zhen Yan (Texas A&M University), and C. R. Dean (City College of New York) for valuable discussions. We thank K. Watanabe and T. Taniguchi for providing h-BN substrates. This work acknowledges support from the W. M. Keck Foundation, the Office of Naval Research (ONR), and the South West Academy of Nanolectronics of the Nanoelectronics Research Initiative. Work at Columbia University was supported by the Center for Re-Defining Photovoltaic Efficiency through Molecular-Scale Control, an Energy Frontier Research Center funded by the U.S. Department of Energy (DOE), Office of Science, Office of Basic Energy Sciences under award DE-SC0001085, National Science Foundation (NSF) grant DMR-1124894, and ONR grant N000141310662. Work at the Institute of High Performance Computing was supported by the Agency for Science, Technology And Research (A*STAR), Singapore. Work at Sandia was supported by the Office of Basic Energy Sciences, Division of Materials and Engineering Sciences, U.S. DOE, under contract no. DE-AC04-94AL85000. Work at Rice University was supported by the ONR and NSF's Chemical, Bioengineering, Environmental, and Transport Systems Division. The first-principles computations were performed on Kraken at the National Institute for Computational Sciences (NSF grant OCI-1053575), Hopper at the National Energy Research Scientific Computing Center (DOE grant DE-AC02-05CH11231), and DaVinCI at Rice University (NSF grant OCI-0959097). H.C. acknowledges support from NSF grant DMR-1122603. A relevant patent application is in process.

Supplementary Materials

www.sciencemag.org/content/342/6159/720/suppl/DC1
Materials and Methods
Supplementary Text
Figs. S1 to S12
References (*32*–*45*)

29 July 2013; accepted 1 October 2013
10.1126/science.1243879

The Role of Surface Oxygen in the Growth of Large Single-Crystal Graphene on Copper

Yufeng Hao *et al.*

Science **342**, 720 (2013);
DOI: 10.1126/science.1243879